Supplementary Information

Layer-dependent ultrafast carrier dynamics of $PdSe_2$ investigated by photoemission electron microscopy

Xiaying Lyu[1], Yaolong Li[1], Xiaofang Li[1], Xiulan Liu[1], Jingying Xiao[1], Weiting Xu[4], Pengzuo Jiang[1], Hong Yang[1,2,3], Chengyin Wu[1,2,3], Xiaoyong Hu[1,2,3], Liangyou Peng[1,2,3], Qihuang Gong[1,2,3], Shengxue Yang[4]*, Yunan Gao[1,2,3]**

[1]State Key Laboratory for Mesoscopic Physics & Department of Physics, Collaborative Innovation Center of Quantum Matter and Frontiers Science Center for Nano-optoelectronics, Beijing Academy of Quantum Information Sciences, Peking University, Beijing 100871, China.

[2]Peking University Yangtze Delta Institute of Optoelectronics, Nantong, Jiangsu 226010, China.

[3]Collaborative Innovation Center of Extreme Optics, Shanxi University, Taiyuan, Shanxi 030006, China.

[4]School of Materials Science and Engineering, Beihang University, Beijing 100191, China

Table of Contents

1. Principle of TR- and ER-PEEM measurements

Schematic of time- and energy-resolved PEEM measurements is shown in Figure S1, where a pump pulse excites ground-state electrons from valence bands to conduction bands, after a time delay Δt, a probe pulse ionizes the excited-state electrons in conduction bands to vacuum state to be collected and imaged. By tuning time delay, the temporal evolution of the population of photoexcited electrons is yielded. Energy slit of hemispherical electron energy analyzer selects electrons with a specific energy level. The temporal and energy resolution of our TR- and ER-PEEM is approximately 200 fs and 150 meV, respectively.

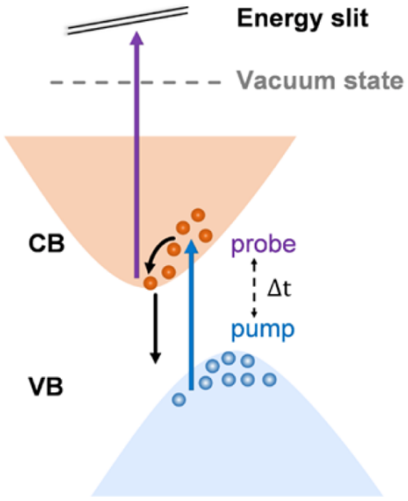

Figure S1. Schematic of TR- and ER-PEEM measurements.

2. Optical microscopy image and atomic force microscopy (AFM) morphology of $PdSe_2$ on h-BN and silicon substrate

Optical microscopy image of $PdSe_2$ on h-BN and silicon substrate is shown in Figure S2a. The light-yellow rectangular background is p-type doped pure silicon substrate, h-BN is within the brownish area (frame in black dashed line), and the topmost bright yellow area represents $PdSe_2$ (frame in red dashed line). Raman spectra of three typical layer thickness of $PdSe_2$ exhibits four apparent peaks at approximately 143 cm^{-1}, 206 cm^{-1}, 222 cm^{-1} and 258 cm^{-1} (corresponding vibration modes: A_g^1, A_g^2, B_{1g} and A_g^3, Figure 1c), and with the increase of layer, the A_g^1 and A_g^3 modes

redshifts gradually similar to previous reports[1], indicating the stronger interlayer coupling. The close-up of AFM scanning morphology is shown in Figure S2c, and the h-BN substrate is about 25 nm (Figure S2d) in height as guided by the red solid line in Figure S2c.

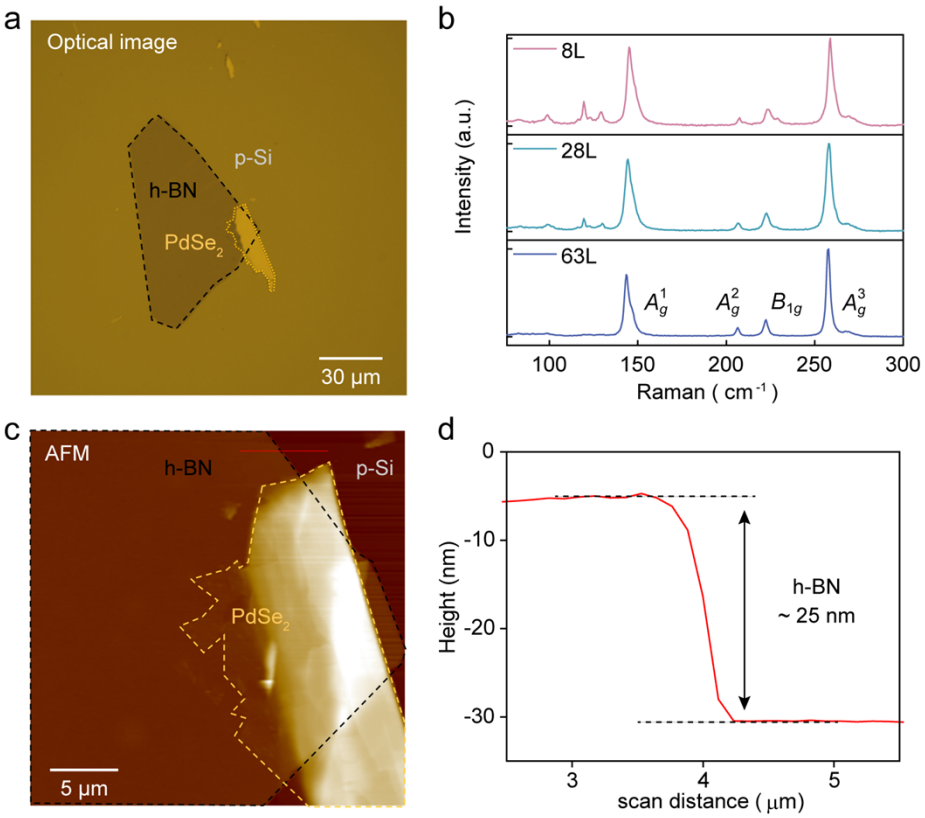

Figure S2. (a) Optical microscopy image of $PdSe_2$ on h-BN and silicon substrate. (b) Raman spectra of $PdSe_2$ nanoflakes with different thickness. (c) The close-up of AFM scanning morphology. (d) Height of h-BN nanoflake in Figure S2c.

3. Photoemission intensity decay trace of $PdSe_2$ with different layer thickness and the magnified AFM scanning morphology of thick-layer $PdSe_2$ nanoflakes

Figure S3a shows the photoemission electron intensity decay trace of $PdSe_2$ with different layer thickness, with background signal subtracted. As seen, due to the linear dichroism transition, interference effect and local background optical field enhancement, the photoemission intensity of $PdSe_2$ nanoflakes don't increase monotonically with different layer thicknesses. Different photoemission electron intensity suggests different carrier concentration, which doesn't influence the electron dynamics in our experiments (Figure 4a). Moreover, Figure S3b exhibits the magnified

AFM scanning morphology (within black dashed line box) of thick-layer $PdSe_2$ nanoflakes. The corresponding layer thicknesses are labeled in different colors.

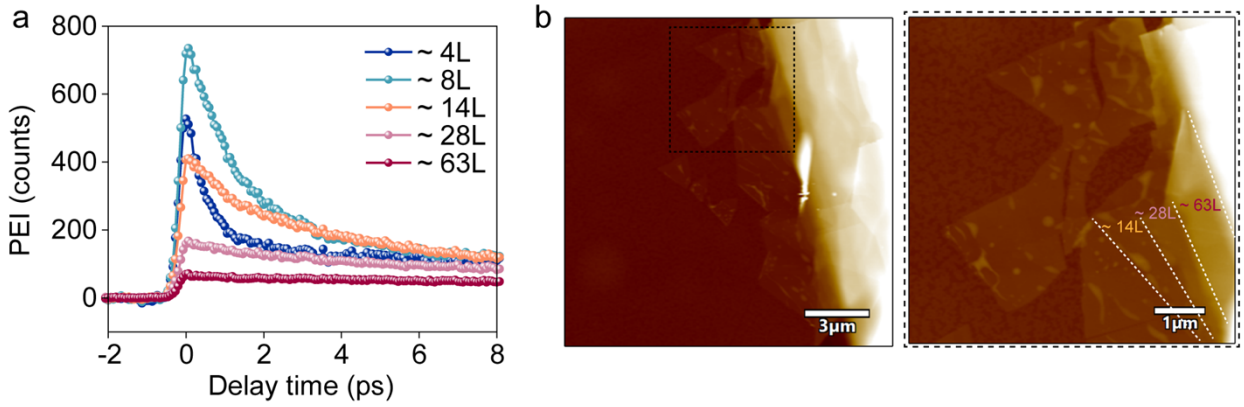

Figure S3. (a) Photoemission electron intensity decay traces of $PdSe_2$ with different layer thickness. (b) The magnified AFM scanning morphology of thick-layer $PdSe_2$ nanoflakes (within black dashed line box).

4. Decay time of the slow decay component with different layer numbers

By fitting with a biexponential decay function convoluted with the instrument response function, the decay time τ_2 of the slow decay component with different layer numbers in Figure 2a are extracted in Figure S4. As shown, for both few-layer and thick-layer $PdSe_2$ nanoflakes, the time constants of slow decay are approximately tens of picoseconds, without an obvious layer-thickness dependence.

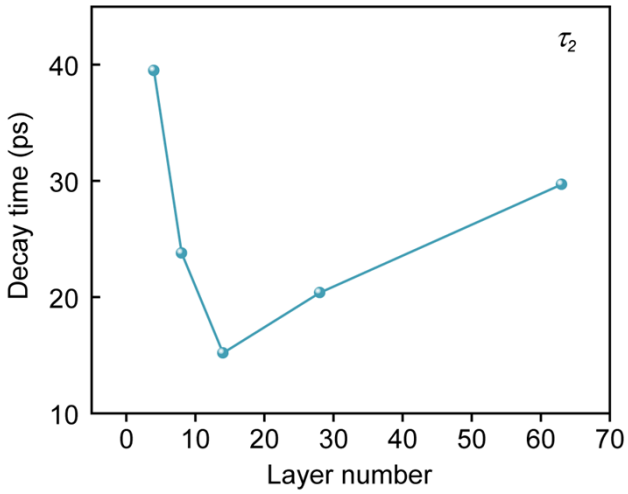

Figure S4. Decay time of the slow decay component with different layer numbers in Figure 2a.

5. Raw photoemission intensity decay trace for $PdSe_2$ on h-BN and silicon substrate

Figure S5 shows raw data of PEI decay traces for ~ 8L $PdSe_2$ and h-BN nanoflake. There is no apparent pump-probe signal of photoemission intensity on h-BN nanoflake, while the ~ 8L $PdSe_2$ displays the maximum intensity at zero point (0 ps). Here, the constant background signal before 0 ps (about 400 counts) mainly come from the excitation by individual single pulse, 273 nm and 410 nm laser pulse, through one-photon or two-photon photoemission process, which is related to light power and exposure time. In the main text, the background signals before 0 ps are subtracted in all decay traces to extract the real pump-probe signals of carrier dynamics.

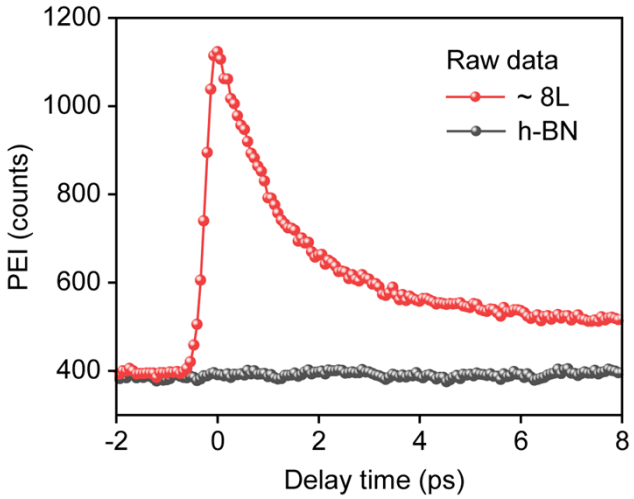

Figure S5. Raw data of photoemission intensity decay traces for ~ 8L $PdSe_2$ and h-BN nanoflake.

6. Electronic band structure of $PdSe_2$ with different layer thicknesses

Figure S6 (a-g) shows the electronic band structure of $PdSe_2$ with 1, 2, 3, 4, 5, 8 layers and bulk state, calculated by density functional theory (DFT) using the Vienna Ab initio Simulation Package (VASP). Theoretically calculated band gaps with different layer thicknesses are collected in Figure S6h. As seen, along with the increase of layer number, the bottom of conduction bands sharply decreases, while the top of the valence band remains nearly unchanged, which causes the significant reduction in the band gap. When the layer thickness increases to tens of layers (about

20 – 30L), conduction bands cross with valence bands, resulting in 0 eV band gap and the transition from semiconductor phase to semimetal phase, which is consistent with previous reports.

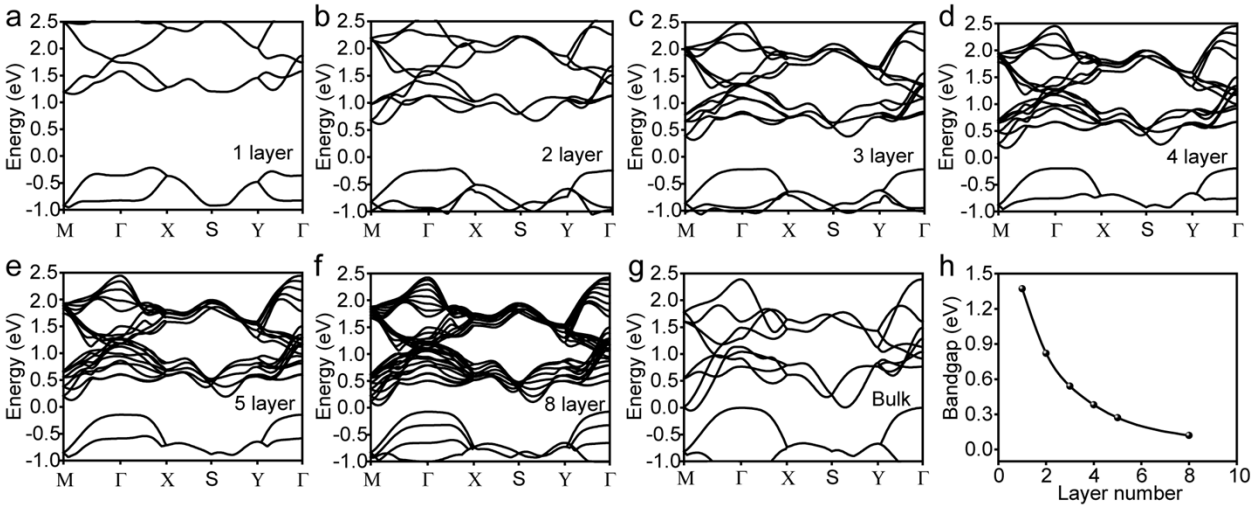

Figure S6. (a-g) Electronic band structure of $PdSe_2$ with different layer thicknesses. (h) Theoretically calculated band gaps of $PdSe_2$ with different layer thicknesses.

7. Photoemission decay traces at high energy peak in EDCs for ~ 8L and ~ 63L $PdSe_2$

Figure S7a and S7b exhibit the photoemission decay traces at high energy peak in EDCs in Figure 3b and 3e, at 0.65 eV (E_2) of ~ 8L $PdSe_2$ and 1.10 eV (E_4) of ~ 63L $PdSe_2$, respectively, normalized by the maximum at 0 ps. By fitting with exponential decay function, an ultrafast decay on a timescale of ~ 0.3 ps at both 0.65 eV (E_2) and 1.10 eV (E_4) is determined, which reflects the ultrafast hot electron cooling from high energy levels to lower ones.

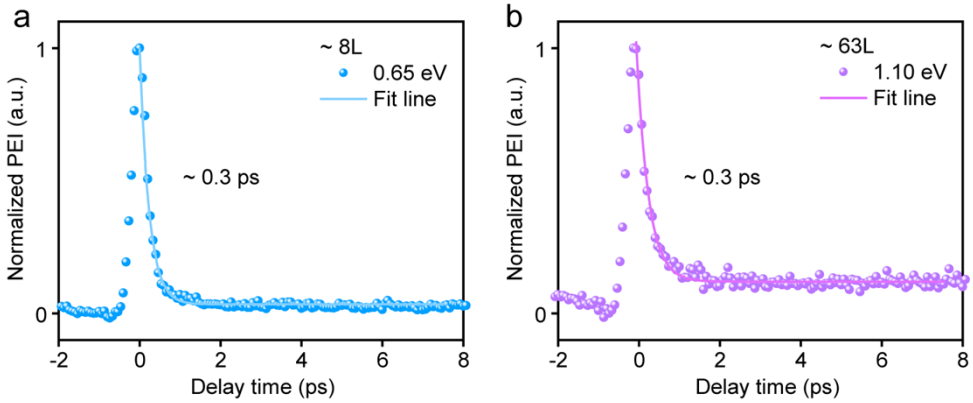

Figure S7. (a, b) Photoemission decay traces at high energy peak in EDCs for ~ 8L and ~ 63L $PdSe_2$ normalized by the maximum at 0 ps.

8. Population of excited-state electrons in the conduction band versus energy and delay time for ~ 14L $PdSe_2$

Evolution of the population of excited-state electrons versus energy and delay time for ~ 14L $PdSe_2$ is depicted in Figure S8a. As the same as ~ 8L and ~ 63L $PdSe_2$ in Figure 3a and 3c, electron energy distribution curves measured with an energy step of 50 meV are presented in Figure S8b, as labeled by horizonal white dashed lines in Figure S8a. Within the first picosecond, the energy peak of EDCs shows redshift from E_6 (0.95 eV) to E_5 (0.75 eV), reflecting the ultrafast hot carrier cooling. The energy difference between high energy peak and low energy peak for ~ 14L $PdSe_2$ is about 0.2 eV, which is reasonable because its bandgap falls between ~ 8L and ~ 63L $PdSe_2$. Moreover, photoemission intensity decay trace at E_5 (0.75 eV) is extracted in Figure S8c. By fitting with exponential decay function convoluted by instrument response function, a fast decay component on a timescale of about 2 ps and a slow decay component of approximately tens of picoseconds (~ 11.4 ps) are determined. The ultrafast decay component of 14 L $PdSe_2$ (~ 2 ps) is attributed to defect trapping process and is slower than that of ~ 8L $PdSe_2$ (~ 1.3 ps), owing to greater thickness and less surface state.

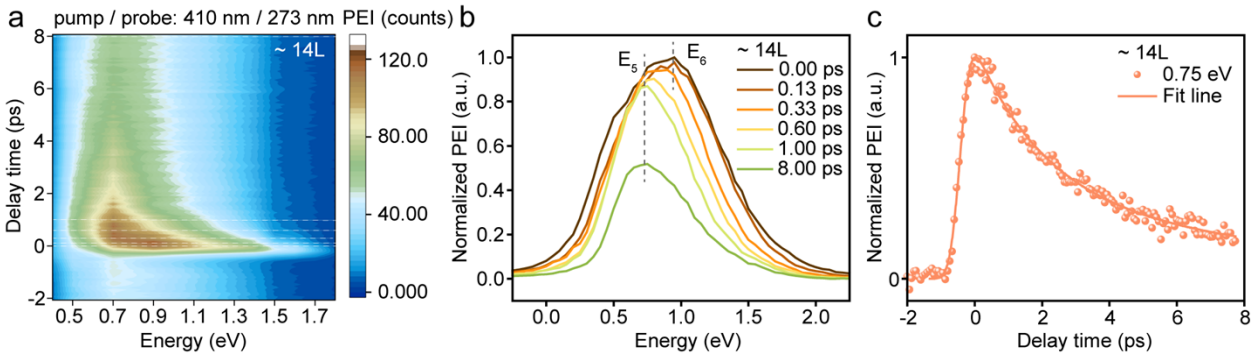

Figure S8. Population of excited-state electrons in the conduction band versus energy and delay time for ~ 14L $PdSe_2$.

9. Pump power-dependent TR-PEEM measurements for few-layer and bulk $PdSe_2$

Figure S9a shows the pump power dependence of photoemission intensity for bulk $PdSe_2$, which shows the same result as ~ 8L $PdSe_2$ in Figure 4a. The laser power of pump pulse doesn't influence the carrier dynamics of few-layer $PdSe_2$ and bulk $PdSe_2$, which only causes a linear change in photoemission intensity (Figure 1d) in current experiments. Furthermore, there are no significant polarization dependence on the carrier dynamics for both few-layer and bulk $PdSe_2$ (Figure 4b and S9b). The photoemission intensity shows little change under the two orthogonal polarization conditions (parallel and vertical to a axis or b axis), possibly due to the little difference in the absorption at different polarizations for both pump and probe pulses.

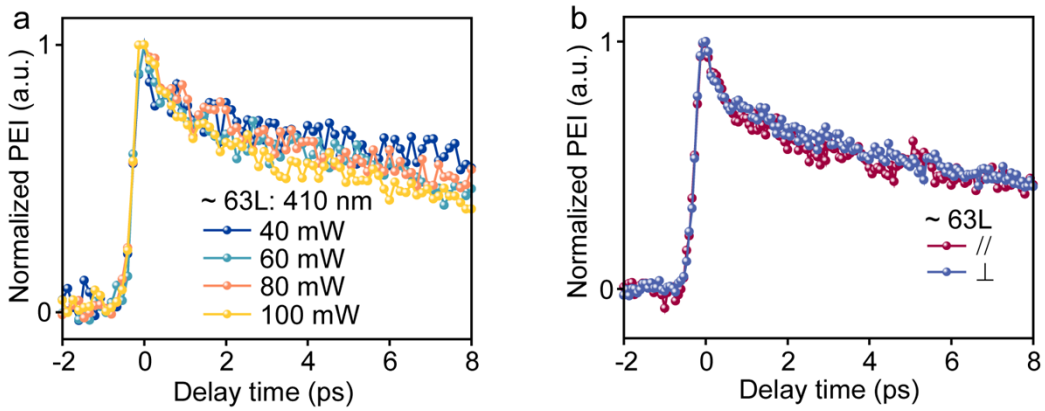

Figure S9. (a) Power-dependence of photoemission intensity for bulk $PdSe_2$. (b) Polarization-dependent carrier dynamics for bulk $PdSe_2$.

Reference

1. L. H. Zeng, D. Wu, S. H. Lin, C. Xie, H. Y. Yuan, W. Lu, S. P. Lau, Y. Chai, L. B. Luo and Z. J. Li, *Adv. Funct. Mater.*, 2019, **29**, 1806878.